Tectonophysics 663 (2015) 302–309

Contents lists available at ScienceDirect

Tectonophysics

journal homepage: www.elsevier.com/locate/tecto

Geodetic evidence for continuing tectonic activity of the Carboneras fault (SE Spain)

Anna Echeverria, Giorgi Khazaradze *, Eva Asensio, Eulalia Masana

RISKNAT Group, Departament de Geodinàmica i Geofísica, Facultat de Geologia, Universitat de Barcelona (UB), Martí i Franquès s/n, 08028 Barcelona, Spain

POSTPRINT

Geodetic evidence for continuing tectonic activity of the Carboneras fault (SE Spain)

Anna Echeverria[1], Giorgi Khazaradze[1], Eva Asensio[1], Eulalia Masana[1]

[1]RISKNAT Group, Departament de Geodinàmica i Geofísica, Facultat de Geologia, Universitat de Barcelona (UB), Martí i Franquès s/n, 08028 Barcelona, Spain

Corresponding author:

Giorgi Khazaradze

Tel: +34934035913

(gkhazar@ub.edu)

Short title: Continuing activity of the Carboneras fault

Keywords: Betic-Rif Arc; Eastern Betic Shear Zone; Carboneras Fault; Crustal deformation; Active faults; Geodynamics; GPS; Seismicity

1. Introduction

GPS geodesy is a useful and efficient tool for identifying tectonically active faults or regions and for quantifying their deformation in terms of slip and strain rates. Several studies based on permanent and non-permanent GPS networks (e.g. Alfaro et al., 2006; Echeverria et al., 2013; Gárate et al., 2014; Gil et al., 2002) and high-precision levelling profiles have been carried out in SE Spain (e.g. Galindo-Zaldívar et al., 2013; Giménez et al., 2000; Marín-Lechado et al., 2005) revealing an on-going tectonic activity of this part of the Iberian Peninsula. However, in many cases the presented results were inconclusive, since at slow deformation rates (<2 mm/yr), a long period of observation is required to obtain statistically significant results.

In this paper, we focus on studying the present-day geodetic slip rate of the Carboneras fault zone (CFZ), which belongs to the NE-SW trending Eastern Betic Shear Zone (EBSZ) located in the SE Spain (Figure 1a). The EBSZ is composed, from north to south, by the Bajo Segura, Carrascoy, Alhama de Murcia, Palomares and Carboneras faults, has been subject to a NNW-SSE oriented shortening with an associated ENE-WSW extension since Miocene time (Alfaro et al., 2008; Galindo-Zaldívar et al., 1999). The compression has resulted in the activation of the several brittle fault zones (Bousquet, 1979) and folding (Galindo-Zaldívar et al., 2003, Figure 1b). The extension is expressed through a number of NW-SE and WNW-ESE oriented normal faults (see for example, AdF and BF faults in Figure 1b), especially in the central Betics (Galindo-Zaldívar et al., 2003) and west of the EBSZ, reaching the Guadix-Baza basin (Alfaro et al., 2008). At the scale of the Iberian Peninsula, the EBSZ absorbs part of the convergence between the Eurasian and Nubian plates (Masana et al., 2004), which is of the order of 4 to 6 mm/yr in the NW direction (e.g. Argus et al., 2011; McClusky et al., 2003; Moreno, 2011; Serpelloni et al., 2007) (Figure 1b). As of CFZ, the previously estimated geologic slip rates for this fault range between 0.05-2 mm/yr, depending on the data used and the covered time-period (Bell et al., 1997; Hall, 1983; Montenat et al., 1990; Moreno, 2011).

The main objective of this paper is to present the contemporary crustal deformation velocity field of the CFZ, with the aim of obtaining slip rates and comparing them to the mid-and-long-term geologic slip rates. The installation of the GATA continuous GPS station has enabled us to obtain continuous observations from both sides of the fault and consequently, to quantify its slip rate. Apart from our preliminary results (Khazaradze et al., 2010; 2014), no quantitative estimates of the present-day geodetic slip rates of the CFZ have been published previously.

2. Active faults and seismicity in the SE Betics

The south-eastern Betic Cordillera has gone through historical damaging earthquakes and shallow instrumental seismicity (Figure 2) with low to moderate magnitude (e.g. Buforn et al., 1995; Stich et al., 2003a). This seismicity is an evidence for the presence of on-going tectonic activity and active faults. The study area has a variety of faults with recent activity (Figure 1), where two types of faults dominate: i) major strike-slip fault zones like the right-lateral Alpujarras (AFZ) (Sanz de Galdeano et al., 1985) and the left-lateral Carboneras (CFZ) fault zones (e.g. Bousquet, 1979; Keller et al., 1995) and ii) normal faults of variable scale, oriented NNW-SSE to NW-SE, such as the Adra (Gràcia et al., 2012), the Balanegra (e.g. Galindo-Zaldívar et al., 2003), and the Loma del Viento (Pedrera et al., 2012b) faults.

The CFZ is one of the longest continuous structures of the EBSZ. The 50-km long emerged portion of the CFZ is cut to the north by the Palomares fault (Gràcia et al., 2006) and continues offshore into the Alboran Sea for 100 km (Figure 1) (Moreno, 2011). The CFZ is a major crustal-scale fault and according to some authors can reach down to the Moho (e.g. Pedrera et al., 2010). Soto et al. (2008) suggest that the CFZ reaches a domain with partial melting in the deepest crust. At surface, the fault has a clear morphologic expression, changing its width along the fault trace from a single narrow trace to a 2 km-wide fault zone (Moreno et al., 2008). Another major strike-slip fault has been defined northwest of the CFZ, namely the Alpujarras fault zone (AFZ), composed by a number of E-W oriented right lateral strike-slip faults located within a wide corridor and forming a transfer fault zone, active since the Miocene (Martínez-Díaz and Hernández-Enrile, 2004; Martínez-Martínez et al., 2006; Sanz de Galdeano et al., 2010). These major strike-slip faults separate domains affected by different structural evolution: the CFZ separates the thinned crust with Neogene volcanics of the Cabo de Gata in the eastern part (Figure 1) from Neogene tilted block domains, consisting of sediments and metamorphic basement of the Internal Betics, in the western block (e.g. Martínez-Díaz and Hernández-Enrile, 2004; Pedrera et al., 2006; Rutter et al., 2012). The AFZ on the other hand, separates the tilted block domain to the south from the Sierra Nevada elongated core-complex to the north (Martínez-Martínez et al., 2006).

The WNW-ESE to NW-SE Quaternary normal faults are encountered across the central and eastern Betics (Galindo-Zaldívar et al., 2003; Marín-Lechado et al., 2005; Pedrera et al., 2006). In addition to WNW-ESE normal faults, Gràcia et al. (2006) described N-S oriented offshore normal faults on the northern block of CFZ. Many of these normal faults are found in the area bounded by the dextral AFZ and the sinistral CFZ (Figure 2). For this reason, several authors (e.g. Giaconia et al., 2014; Martínez-Díaz and Hernández-Enrile, 2004; Martínez-Martínez et al., 2006; Sanz de Galdeano et al., 2010) have suggested that the CFZ and the AFZ strike-slip faults act in conjunction with the normal faults. The CFZ and/or the AFZ have been interpreted as deeper transfer faults accommodating heterogeneous extension due to the shallower normal faults (Giaconia et al., 2014; Martínez-Martínez et al., 2006). Martínez-Díaz and Hernández-Enrile (2004) proposed a kinematic model, where a tectonic block bounded by both strike-slip faults escapes to the west, thus relating local extensional structures to the compressive tectonics.

The historical seismicity record of the EBSZ shows the presence of damaging earthquakes with MSK intensities of VIII-IX. Some of the notable examples include destructive earthquakes that affected the city of Almeria in 1522 (I=VIII-IX), 1658 (I= VIII) and 1804 (I=VIII). The shallow (< 50 km depth) instrumental seismicity, covering a time period from 1926 to 2013, is characterized by low magnitude earthquakes, with no event larger than M_w5.0 (IGN catalogue, www.ign.es) (Figure 2). These earthquakes are usually related to minor faults (e.g. Martínez-Díaz and Hernández-Enrile, 2004) located within the crustal blocks bounded by the major strike-slip faults (Figure 2). Rodríguez-Escudero et al. (2013) interpret the events with M_w<5 as part of the background seismicity, which can occur at any point within the crustal blocks bounded by the large E-W to NE-SW strike-slip faults. Precisely along these major faults (i.e. CFZ or AFZ) is where earthquakes of Mw>5.5 are expected by these authors. The instrumental and historical seismicity related to the CFZ is scarce, apart from the 1522 Almería (MSK I=VIII-IX) earthquake that has been tentatively assigned to the Carboneras fault offshore section (Reicherter and Hübscher, 2007; Moreno, 2011). Recent paleoseismological studies (Gràcia et al., 2006; Moreno, 2011) provided evidence for the seismogenic nature of the CFZ based on the occurrence of surface rupturing earthquakes during late Pleistocene and Holocene.

To facilitate the interpretation of the seismo-tectonic activity in the SE Betics, a database of earthquake moment tensors based on available literature and public catalogues was compiled (see Figure 2 and Table A1). The master catalogue used was the IAG Regional Moment Tensor catalogue (Stich et al., 2003a, 2006, 2010), since it was specifically created to perform time-domain moment tensor inversion of small to moderate events (m_b >3.5) in the Ibero-Maghreb region. In the cases where only the fault plane solutions were available, we used the MoPaD software (Krieger and Heimann, 2012) to obtain the moment tensor. The final catalogue has 37 focal mechanisms, from 1910 to 2013, with magnitudes ranging from M_w3.3 to 6.1. The 1910 Adra M_w6.1 earthquake (Stich et al., 2003b), the largest event in the catalogue, accounts for 90% of the total seismic moment release in the area. A majority of the focal mechanisms indicate normal or strike-slip kinematics (or a combination of both). The orientation of P and T axes, obtained with ObsPy software (Beyreuther et al., 2010) is similar for all the events (Figure 2). The average P axis is oriented N338º (NNW-SSE), roughly parallel to the plate convergence vector (Figure 1), while the T axis has an average orientation of ENE-WSW (N68º), compatible with the NW-SE striking normal faults.

3. GPS data and analysis

The geodetic study was carried out with continuous GPS stations (CGPS), including the new stations GATA (University of Barcelona), and two Topo-Iberia network stations: NEVA (installed in October 2008) and PALM (installed in June 2008) and survey mode GPS stations (SGPS) located in the study area belonging to the CuaTeNeo network. The CuaTeNeo geodetic network was built in 1996 and has been observed 5 times: 1997, 2002, 2006, 2009 and 2011 (Echeverria et al., 2013). The GATA continuous GPS station was installed in December 2008 as part of the *EVENT* Project with the specific objective of quantifying the present-day slip-rates of the CFZ (Khazaradze et al., 2010). The station was installed 2 km SW from the village of Rodalquilar in the Sierra de Cabo de Gata, ~200m from CuaTeNeo campaign monument RELL. The GATA monumentation consists of the short drill brace type monument designed by UNAVCO (Figure 3), with 4 solid stainless steel rods, anchored at least half a meter into the bedrock (Miocene volcanic rocks). This type of monumentation ensures a good long-term stability of the station. The monument is equipped with the SCIGN type antenna adapter and a dome. The hardware includes the Leica GRX1200+GNSS receiver and the AT504GG choke-ring antenna, powered by an 80-watt solar panel. Since 2011, the station has experienced hardware problems, related to the malfunction of the solar power system and GPRS modem (see gaps in the time series in Figure 3).

In total, we processed 4.5 yr data from 75 continuously recording GPS (CGPS) stations located both in the eastern Betics and throughout Eurasia and Africa. GPS data were processed using GAMIT/GLOBK software 10.4 (Herring et al., 2010). The data analysis methodology is described in detail in Echeverria et al. (2013) and Asensio et al. (2012). The time-span of the analysed data was nearly uniform, from 2008.8 to 2013.3, which equals to 4.5 yr of observations. According to Blewitt and Lavallé (2002) this time-span is sufficient to appropriately model the annual oscillations in the resulting time-series and achieve an optimal resolution in the velocity estimates. The formal errors were obtained firstly by removing the annual signal and secondly by applying the Real Sigma (RS) algorithm implemented in the GLOBK module (Herring, 2003). As a result, to obtain the final velocity solution and the error estimate, the estimated random walk through the RS algorithm was included for each component of the individual station (Reilinger et al., 2006; Shen et al., 2011). In order to validate the formal errors we compared the resulting uncertainties with the uncertainties calculated using the

CATS software (Williams, 2008), where we estimate velocity uncertainties from the time-series using a model of an annual term, white noise and flicker noise. The mean difference between both models is 0.04 mm/yr for CGPS stations components for which the CATS analysis produced a valid estimate of uncertainty.

The obtained ITRF2008 velocity field was rotated to western Europe reference frame as defined by Echeverria et al. (2013). The rotation was performed using the Velrot program included in GAMIT/GLOBK package (see stations in common used for the rotation in Table A2). The Velrot was also used to combine the SGPS station velocities of Echeverria et al. (2013) with the CGPS velocity field. The resulting average root mean square of the combination is 0.28 mm/yr, indicating a good adjustment.

4. Results

The present-day horizontal velocity field in the region of the Carboneras fault is shown in Figure 4 with numerical results provided in Table A2. The estimated velocities range between 1.1 and 3.1 mm/yr. As expected, the stations located closer to the Nubia/Eurasia plate boundary, along the coast, move faster than the stations located farther inland (CUCO, CAAL and NEVA). As mentioned earlier, the overall convergence rate between the Nubia/Eurasia plates is 4 to 6 mm/yr, which means that a significant portion of this overall budget is being accommodated within the study area.

The most important feature of the obtained velocity field is a significant change in the orientation of the calculated velocities from east to west (Figure 4). In the western Europe reference frame, the easternmost stations move at rates of 1.3-2.0 mm/yr in the direction of the Nubia (i.e. Africa)-Eurasia convergence. Stations located to the west, starting from HUEB SGPS station, show a more westerly-south-westerly motion, exhibiting a counter-clockwise rotation. The westernmost PALM and MOTR CGPS stations show the highest velocities (2.8±0.1 and 3.1±0.1 mm/yr, respectively) with SW direction (Figure 4 and Table A2). In respect to the CFZ, the stations of the eastern block of CFZ move at 1.6-1.8 mm/yr with an azimuth of 325º (with respect to the western Europe reference frame), while the western block stations move at a rate of 1.5-1.9 mm/yr in an average direction of 280º. To assess the present-day slip-rates related to the CFZ we have constructed a CFZ trace perpendicular velocity profile (azimuth N138ºE) shown in Figures 4 and 5. Although there are only a few stations at each side of the fault, the differential motion between each group is evident and can be estimated. To derive the geodetically estimated slip rate we assume that the differential motion between the two groups of stations, located on each side of the CFZ, is related solely to the CFZ. By projecting the velocities to the profile parallel and perpendicular direction, we attempt to estimate the compressive or extensive (ΔV_c) and strike-slip (ΔV_{ss}) fault slip-rate components, respectively. Despite the presence of NW-SE normal faults and E-W to ENE-WSW folds (Pedrera et al., 2012a), to calculate the fault slip rate we assume that each block is rigid, without any internal deformation. This assumption is supported by the fact that the velocities of various stations located at each side of the fault are almost identical. Only the strike-slip component shows a significant differential motion across the CFZ (Figure 5). Taking into account the velocity errors, we obtain a minimum and maximum values for ΔV_{ss} of 1.1 to 1.5 mm/yr, which are equivalent to an average present-day strike-slip rate of 1.3±0.2 mm/yr. The fault-normal (i.e. profile parallel) component (ΔV_c) across the CFZ is statistically insignificant.

5. Discussion

In this work, for the first time, we were able to quantify the present-day horizontal crustal deformation rates across the CFZ, using continuous and campaign GPS observations conducted during the last decade. Almost identical velocity vectors observed at two closely located stations, GATA (CGPS, 4.5 yr processed) and RELL (SGPS, 15 yr processed, Figure A3), evidence the high accuracy of the presented results. This good agreement between the two independent observations also reaffirms the usefulness of the campaign-style GPS observations, even when the deformations are slow, like in eastern Betics.

The obtained horizontal velocity field for the SE Betics confirms the continuing tectonic activity of the on-shore segment of the CFZ. We find that the left-lateral motion dominates the kinematics of the CFZ at rate of 1.3±0.2 mm/yr along N48º direction. The shortening component is significantly lower and poorly constrained. Thus, the GPS measurements suggest a dominance of the strike-slip motion in the transpressional kinematics of the CFZ, coherent with the positive flower structure observed in La Serrata (e.g. Moreno, 2011; Reicherter and Reiss, 2001). The GPS derived geodetic fault slip rates presented here can be considered as maximum values, since we assumed that all the observed differential motion is solely due to the CFZ and distributed deformation along secondary faults was not considered. We have also assumed that the entire on-shore CFZ moves with the same slip rate and ignored the possibility of along-strike variations. With a denser GPS coverage, it would have been possible to provide an estimate of this variability and to confirm whether or not the easternmost segment with almost no differential motion between CUCO-MOJA and CARB is inactive.

The most recent study, integrating both onshore and offshore paleoseismic and geomorphologic results, using the youngest faulted features, suggest the lower bound for the Quaternary strike-slip rate of 1.1 mm/yr (Moreno, 2011). This result is in good agreement with the geodetic slip rates presented in this work, suggesting that most of the deformation registered by GPS can be attributed solely to the activity of the CFZ. Combining the geologic (minimum values) and geodetic (maximum values) slip rates, we can conclude that the long-term strike-slip rate of the CFZ must be enclosed between the minimum geologic slip rate of 1.1 mm/yr and the maximum geodetic slip rate of 1.5 mm/yr.

We calculated the strain rate field (Figure 6) by the inversion of the GPS data using SSPX software (Cardozo and Allmendinger, 2009) for the 6 GPS stations located at both sides of the CFZ. Horizontal principal strain rate axes obtained at the centre of these 6 stations show a predominance of a compressive strain rate: $\dot{\varepsilon}_{min}$= -26.2±8 nstrain/yr oriented N354º. The extensional component is lower: $\dot{\varepsilon}_{max}$= 18.1±7 nstrain/yr with an azimuth of N84º. The orientation of the geodetic compressive and extensive strain rate axes is in agreement with the N338º and N68º orientation of the mean P-T axes obtained from the earthquake focal mechanisms (Figure 2). The resulting left-lateral shear plane of the maximum shear strain rate ($\dot{\varepsilon}_{sh-max}$) has an orientation of N39º, sub-parallel to the CFZ trace (N48º). Unfortunately, due to the sparse spatial distribution of GPS stations, we cannot discern with certainty whether the accumulated strain is released aseismically (e.g. creep) or the fault is locked and is being loaded for the occurrence of the earthquake. However, taking into account the paleoseismological results that point to repetitive large paleoearthquakes along the CFZ (e.g. Gràcia et al., 2006; Moreno, 2011), a locked fault scenario seems more plausible. In contrast, Faulkner et al. (2003) suggested a mixed mode fault slip behaviour (when fault creep is interspersed with seismic locking) for the CFZ, drawing an analogy with the Parkfield section of the San Andreas fault. The clarification of the seismic or aseismic behaviour of the CFZ is crucial for seismic hazard calculations in this region and thus, the future studies should include the densification of the measurements.

The north-eastern termination of the CFZ continues into the Palomares fault (PF), a sinistral strike-slip fault oriented N-S (Figures 1 and 6). Given the current distribution of the GPS points, especially the absence of points on the eastern side of the PF, we are unable to quantify the current activity of this fault. However, it should be mentioned that some authors do attribute a tectonic activity to the PF, but the suggested slip-rates are of the order of sub-millimetre per year (e.g. Booth-Rea et al., 2004; García-Mayordomo and Jiménez-Díaz, 2010) and are not detectable using the GPS technology.

The kinematics of the CFZ is better observed by fixing the GATA station (Figure 6). This way, the resulting GPS velocities show a clearly opposite sense of kinematics across the Alpujarras and the Carboneras fault zones. The former shows right-lateral motion (CAAL-CUCO stations move to the south while HUEB moves to the south-west), while the latter shows left-lateral motion (compare GATA-RELL to HUEB-ALMR-ALME stations). With the current spatial GPS distribution along the AFZ it is impossible to characterize possible along-strike velocity variations. In the proposed simplified kinematic model (Figure 7), we treat AFZ as a continuous fault, although we are conscious that this corridor is composed by several E-W oriented individual fault segments. This simplification also ignores the fact that some of these segments seem to be inactive (e.g. Pedrera et al., 2012a). Martínez-Díaz and Hernández-Enrile (2004) proposed that this type of movement of the AFZ and CFZ induces a westward tectonic escape of the wedge bounded by these two strike-slip faults (Figure 7). According to them, deformation gradient in the escaping block favours the formation or reactivation of NNW-SSW normal faults perpendicular to the east-west extensional motion of the block. Our GPS results clearly show an increase in the observed velocity magnitudes of the escaping block for the westerly group (PALM and MOTR) with respect to the easterly stations (HUEB, ALME and ALMR) (Figures 4 and 6). This observation is in agreement with the escaping block model proposed by the authors. Although the absence of data in-between the two groups, prevents the clarification of the exact nature of strain repartitioning. However, the picture is more complex. East-to-west increase in the southward motion of the stations located north of the AFZ in GATA fixed reference frame (compare NEVA with CAAL or CUCO in Figure 6) and an apparent counter-clockwise rotation of the stations belonging to the escaping block (compare the stations GATA, HUEB, ALME, PALM and MOTR in Figures 4 and 6) cannot be satisfactorily explained solely by the convergence of the Nubia plate, resulting in a block escape. Simple *push* cannot cause the above-mentioned rotation and acceleration in the GPS velocities. For this reason, we hypothesize that an additional *pulling* force must exist in order to satisfactorily explain the observed crustal deformation pattern. Considering the proximity of the oceanic slab in depth (Figure 1a), which is located further west and possibly attached to the continental crust in central Betics and eastern Rif (e.g. Bonnin et al., 2014), sub-lithospheric processes such as a rollback of the subducting slab, can hypothetically be responsible for such a pull. An observed change in the motion of the GPS velocities, starting from the location of station HUEB (2.5°W, Figures 4 and 6), coincides approximately with the area where a significant east-to-west increase of the lithospheric thickness is deduced from seismic studies (Levander et al., 2014). On a more regional scale, Pérouse et al. (2010), combined GPS data with numerical modelling, and suggested a combined effect of plate convergence, low rigidity of the Alboran Sea region and a S-SW directed traction related to sub-lithospheric processes, as an explanation for the regional geodynamics. In this simplified kinematic model (Figure 7), we propose that the Carboneras fault zone acts as a boundary between the eastern block that moves parallel to the plate convergence vector and the western block that moves westward due to the block escape and deeper sub-lithospheric processes. For this reason, an area affected by deeper sub-lithospheric processes (shaded region in Figure 7) does not extend south of the CFZ. This assumption can be supported by the description of the CFZ as a major crustal-scale fault that reaches the Moho (e.g. Pedrera et al., 2010).

6. Conclusions

The analysis of GPS data in the SE Betics confirm and quantify the on-going tectonic activity of the onshore segment of the CFZ as a left-lateral strike-slip fault. For the first time, we were able to provide a quantitative measure of the present-day horizontal geodetic slip-rate of the CFZ, suggesting a maximum left-lateral motion of 1.3±0.2 mm/yr. The coincidence of geologic and geodetic strike-slip rates along the CFZ, illustrates how during Quaternary its northern segment has been tectonically active and has been slipping at a rate of 1.1 to 1.5 mm/yr. Further investigations should concentrate in determining the nature of the strain accumulation along the CFZ (e.g. creep vs. locking), since this question is crucial for a better estimation of the seismic hazard in the area.

The presented GPS measurements also corroborate that the eastern Alpujarras fault zone (AFZ) is active and exhibits a right-lateral motion. These opposite type strike-slip motion across the AFZ and CFZ is a result of a push-type force due to Nubia and Eurasia plate convergence, that results in the westward escape of the block bounded by these two faults. In addition, due to the observed gradually increasing westerly motion and counter-clockwise rotation of the GPS stations located west of longitude 2.5°W, we propose the existence of additional pull-type forces related to deep sub-lithospheric processes. The implications of the presented results and the simplified kinematic model in terms of the regional geodynamics will require further investigations, that should employ the densification of the GPS observations, combination of various geophysical and geological data, as well, as numerical modelling.

Acknowledgments

The Topo-Iberia (CSD2006-00041), EVENT (CGL2006-12861-C02-01) and CuaTeNeo (CGL2004-21666-E) projects of the Spanish government funded this research. A. E. was supported by the APIF pre-doctoral grant of the University of Barcelona, and E. A. by the FPU pre-doctoral grant (AP-2008-01482) of the Spanish Ministry of Education. We would also like to acknowledge the institutions responsible for the operation of the continuous GPS stations: IGN, ROA, EUREF, IGS, RAP. We thank the Cabo de Gata-Níjar Nature Park administration for their collaboration. Most graphics are from GMT software (Wessel and Smith, 1991). We are thankful to Klaus Reicherter for his helpful comments on the earlier version of this manuscript. The constructive reviews of Dr. Antonio Azor, Dr. Antonio Pedrera and an anonymous reviewer greatly contributed to the improvement of this work.

References

Alfaro, P., Delgado, J., de Galdeano, C.S., Galindo-Zaldívar, J., García-Tortosa, F.J., López-Garrido, A.C., López-Casado, C., Marín-Lechado, C., Gil, A., Borque, M.J., 2008. The Baza Fault: a major active extensional fault in the central Betic Cordillera (south Spain). Int. J. Earth Sci. 97(6), 1353-1365. http://dx.doi.org/10.1007/s00531-007-0213-z.

Alfaro, P., Estévez, A., Blázquez, E.B., Borque, M.J., Garrido, M.S., Gil, A.J., Lacy, M.C., Ruiz, A.M., Giménez, J., Molina, S., Rodríguez-Caderot, G., Ruiz-Morales, M., Sanz de Galdeano, C., 2006. Geodetic Control of the Present Tectonic Deformation of the Betic Cordillera (Spain), in: Sansò, F., Gil, A.J. (Eds.), Geodetic Deformation Monitoring: From Geophysical to Engineering Roles. Springer Berlin Heidelberg, pp. 209-216.

Argus, D.F., Gordon, R.G., Demets, C., 2011. Geologically current motion of 56 plates relative to the no-net-rotation reference frame. Geochem. Geophys. Geosyst. 12(11). http://dx.doi.org/10.1029/2011GC003751.

Asensio, E., Khazaradze, G., Echeverria, A., King, R.W., Vilajosana, I., 2012. GPS studies of active deformation in the Pyrenees. Geophys. J. Int. 190(2), 913-921. http://dx.doi.org/10.1111/j.1365-246X.2012.05525.x.

Bell, J.W., Amelung, F., King, G.C.P., 1997. Preliminary late quaternary slip history of the Carboneras fault, southeastern Spain. J. Geodyn. 24(1-4), 51-66.

Beyreuther, M., Barsch, R., Krischer, L., Megies, T., Behr, Y., Wassermann, J., 2010. ObsPy: A Python Toolbox for Seismology. Seismol. Res. Lett. 81(3), 530-533. http://dx.doi.org/10.1785/gssrl.81.3.530.

Blewitt, G., Lavallée, D., 2002. Effect of annual signals on geodetic velocity. J. Geophys. Res. 107(7), 9-1. http://dx.doi.org/10.1029/2001JB000570

Bonnin, M., Nolet, G., Villaseñor, A., Gallart, J., Thomas, C., 2014. Multiple-frequency tomography of the upper mantle beneath the African/Iberian collision zone. Geophys. J. Int. 198(3), 1458-1473. http://dx.doi.org/10.1093/gji/ggu214.

Booth-Rea, G., Azañón, J.M., Azor, A., García-Dueñas, V., 2004. Influence of strike-slip fault segmentation on drainage evolution and topography. A case study: The Palomares Fault Zone (southeastern Betics, Spain). J. Struct. Geol. 26(9), 1615-1632. http://dx.doi.org/10.1016/j.jsg.2004.01.007.

Bousquet, J.C., 1979. Quaternary strike-slip faults in southeastern Spain. Tectonophysics 52, 277-286. http://dx.doi.org/10.1016/0040-1951(79)90232-4.

Buforn, E., Sanz de Galdeano, C., Udías, A., 1995. Seismotectonics of the Ibero-Maghrebian region. Tectonophysics 248(3-4), 247-261. http://dx.doi.org/10.1016/0040-1951(94)00276-F.

Cardozo, N., Allmendinger, R.W., 2009. SSPX: A program to compute strain from displacement/velocity data. Computers and Geoscinces 35(6), 1343-1357. http://dx.doi.org/10.1016/j.cageo.2008.05.008.

Echeverria, A., Khazaradze, G., Asensio, A., Gárate, J., Dávila, J.M., Suriñach, E., 2013. Crustal deformation in eastern Betics from CuaTeNeo GPS network. Tectonophysics 608, 600-612. http://dx.doi.org/10.1016/j.tecto.2013.08.020.

Faulkner, D.R., Lewis, A.C., Rutter, E.H., 2003. On the internal structure and mechanics of large strike-slip fault zones; field observations of the Carboneras Fault in southeastern Spain. Tectonophysics 367(3-4), 235-251. http://dx.doi.org/10.1016/S0040-1951(03)00134-3.

Galindo-Zaldívar, J., Borque, M.J., Pedrera, A., Marín-Lechado, C., Gil, A.J., López-Garrido, A.C., 2013. Deformation behaviour of the low-rate active Balanegra Fault Zone from high-precision levelling (Betic Cordillera, SE Spain). J. Geodyn. 71, 43-51. http://dx.doi.org/10.1016/j.jog.2013.07.003.

Galindo-Zaldívar, J., Gil, A.J., Borque, M.J., González-Lodeiro, F., Jabaloy, A., Marin-Lechado, C., Ruano, P., Sanz de Galdeano, C., 2003. Active faulting in the internal zones of the central Betic Cordilleras (SE, Spain) J. Geodyn. 36(1-2), 239-250. http://dx.doi.org/ 10.1016/S0264-3707(03)00049-8.

Galindo-Zaldívar, J., Jabaloy, A., Serrano, I., Morales, J., González-Lodeiro, F., Torcal, F., 1999. Recent and present-day stresses in the Granada Basin (Betic Cordilleras): Example of a late Miocene-present-day extensional basin in a convergent plate boundary. Tectonics 18, 686-702. http://dx.doi.org/ 10.1029/1999TC900016.

Gárate, J., Martin-Davila, J., Khazaradze, G., Echeverria, A., Asensio, E., Gil, A.J., de Lacy, M.C., Armenteros, J.A., Ruiz, A.M., Gallastegui, J., Alvarez-Lobato, F., Ayala, C., Rodríguez-Caderot, G., Galindo-Zaldívar, J., Rimi, A., Harnafi, M., 2014. Topo-Iberia project: CGPS crustal velocity field in the Iberian Peninsula and Morocco. GPS Solutions, 1-9. http://dx.doi.org/10.1007/s10291-014-0387-3.

García-Mayordomo, J., Insua-Arévalo, J.M., Martínez-Díaz, J.J., Jiménez-Díaz, A., Martín-Banda, R., Martín-Alfageme, S., Álvarez-Gómez, J.A., Rodríguez-Peces, M., Pérez-López, R., Rodríguez-Pascua, M.A., Masana, E., Perea, H., Martín-González, F., Giner-Robles, J., Nemser, E.S., Cabral, J., 2012. The Quaternary active faults database of Iberia (QAFI v.2.0). J. Iberian Geol. 38(1), 285-302. http://dx.doi.org/10.5209/rev_JIGE.2012.v38.n1.39219.

García-Mayordomo, J., Jiménez-Díaz, A., 2010. Palomares: Carboneras-Sierra de Almenara (ES609), In: Quaternary Active Faults Database of Iberia v.2.0 - December 2011 (García-Mayordomo et al., eds.), IGME, Madrid.

Giaconia, F., Booth-Rea, G., Martínez-Martínez, J.M., Azañón, J.M., Storti, F., Artoni, A., 2014. Heterogeneous extension and the role of transfer faults in the development of the southeastern Betic basins (SE Spain). Tectonics, 33. http://dx.doi.org/10.1002/2014tc003681.

Gil, A.J., Rodriguez, C.G., Lacy, M.C., Ruiz, A.M., Sanz, d.G.C., Alfaro, P., 2002. Establishment of a non-permanent GPS network to monitor the recent NE-SW deformation in the Granada Basin (Betic Cordillera, southern Spain). Studia Geophysica et Geodetica 46(3), 395-410. http://dx.doi.org/310.1023/A:1019530716324.

Giménez, J., Suriñach, E., Goula, X., 2000. Quantification of vertical movements in the eastern Betics (Spain) by comparing levelling data. Tectonophysics 317, 237-258. http://dx.doi.org/10.1016/S0040-1951(99)00318-2.

Gràcia, E., Bartolomé, R., Lo Iacono, C., Moreno, X., Stich, D., Martínez-Diaz, J.J., Bozzano, G., Martínez-Loriente, S., Perea, H., Diez, S., 2012. Acoustic and seismic imaging of the Adra Fault (NE Alboran Sea): in search of the source of the 1910 Adra earthquake. Nat. Hazards Earth Syst. Sci. 12, 3255-3267. http://dx.doi.org/10.5194/nhess-12-3255-2012.

Gràcia, E., Pallas, R., Soto Juan, I., Comas, M., Moreno, X., Masana, E., Santanach, P., Diez, S., Garcia, M., Danobeitia, J., Bartolome, R., Farran, M., Gomez, M., Alpiste, M.J.R., Lastras, G., Wilmott, V., Perea, H., Blondel, P., Gomez, O., Bullock, L., Jacobs, C., Rouse, I., White, D., Whittle, S., Terrinha, P., Gafeira, J., Roque, C., Hits Scientific Party, I., 2006. Active faulting offshore SE Spain (Alboran Sea); implications for earthquake hazard assessment in the southern Iberian margin. Earth Planet. Sci. Lett. 241(3-4), 734-749. http://dx.doi.org/10.1016/j.epsl.2005.11.009.

Hall, S.H., 1983. Post Alpine tectonic evolution of SE Spain and the structure of fault gouges. PhD Thesis, Imperial College London (University of London)

Herring, T., 2003. MATLAB Tools for viewing GPS velocities and time series. GPS Solutions 7(3), 194 - 199. http://dx.doi.org/10.1007/s10291-003-0068-0.

Herring, T.A., King, R.W., McClusky, S.C., 2010. Introduction to GAMIT/GLOBK. Department of Earth, Atmospheric, and Planetary Sciences. Massachusetts Institute of Technology, p. 48

Keller, J.V.A., Hall, S.H., Dart, C.J., McClay, K.R., 1995. The geometry and evolution of a transpressional strike-slip system; the Carboneras Fault, SE Spain. J. Geol. Soc. London 152 (2), 339-351. http://dx.doi.org/10.1144/gsjgs.152.2.0339.

Khazaradze, G., Moreno, X., Asensio, E., & Masana, E. (2010). Geodetic evidence for a present-day activity of the Carboneras fault in the Eastern Betics. In J. M. Insúa & F. Martín-González (Eds.), Contribución de la Geología al Análisis de la Peligrosidad Sísmica (pp. 93–96). Madrid, Spain: IGME.

Khazaradze G., Echeverria A., Asensio E. (2014) Present-day crustal deformation field of the Iberian Peninsula estimated by GPS measurements. Física la Tierra 26:35–46. http://dx.doi.org/10.5209/rev_FITE.2014.v26.46970.

Krieger, L., Heimann, S., 2012. MoPaD - Moment Tensor Plotting and Decomposition: A Tool for Graphical and Numerical Analysis of Seismic Moment Tensors. Seismol. Res. Lett. 83(3), 589-595. http://dx.doi.org/10.1785/gssrl.83.3.589.

Levander, A., Bezada, M.J., Niu, F., Humphreys, E.D., Palomeras, I., Thurner, S.M., Masy, J., Schmitz, M., Gallart, J., Carbonell, R., Miller, M.S., 2014. Subduction-driven recycling of continental margin lithosphere. Nature 515(7526), 253-256. http://dx.doi.org/10.1038/nature13878.

Marín-Lechado, C., Galindo-Zaldívar, J., Rodríguez-Fernández, L.R., Serrano, I., Pedrera, A., 2005. Active faults, seismicity and stresses in an internal boundary of a tectonic arc

(Campo de Dalías and Níjar, southeastern Betic Cordilleras, Spain). Tectonophysics 396(1-2), 81-96. http://dx.doi.org/10.1016/j.tecto.2004.11.001.

Martínez-Díaz, J.J., Hernández-Enrile, J.L., 2004. Neotectonics and morphotectonics of the southern Almería region (Betic Cordillera-Spain) kinematic implications. Int. J. Earth Sci. 93(2), 189-206. http://dx.doi.org/10.1007/s00531-003-0379-y.

Martínez-Martínez, J.M., Booth-Rea, G., Azañón, J.M., Torcal, F., 2006. Active transfer fault zone linking a segmented extensional system (Betics, southern Spain): Insight into heterogeneous extension driven by edge delamination. Tectonophysics 422(1-4), 159-173. http://dx.doi.org/10.1016/j.tecto.2006.06.001.

Masana, E., Martínez-Díaz, J.J., Hernández-Enrile, J.L., Santanach, P., 2004. The Alhama de Murcia fault (SE Spain), a seismogenic fault in a diffuse plate boundary: Seismotectonic implications for the Ibero-Magrebian region. J. Geophys. Res. 109(B01301). http://dx.doi.org/10.1029/2002JB002359.

McClusky, S., Reilinger, R., Mahmoud, S., Ben Sari, D., Tealeb, A., 2003. GPS constraints on Africa (Nubia) and Arabia plate motions. Geophys. J. Int. 155(1), 126-138. http://dx.doi.org/10.1046/j.1365-246X.2003.02023.x.

Montenat, C., D'Estevou, P.O., La Chappelle, G., 1990. Le Bassin de Nijar-Carboneras et le Couloir du Bas-Andarax, Documents et Travaux. Intitute de Geologique Albert de Lapparent 12, 129-164.

Moreno, X., 2011. Neotectonic and Paleoseismic Onshore-Offshore integrated study of the Carboneras Fault (Eastern Betics, SE Iberia). PhD thesis, Universitat de Barcelona, Barcelona, pp. 365. http://www.tdx.cat/handle/10803/77873.

Moreno, X., Masana, E., Gràcia, E., Bartolomé, R., Piqué-Serra, O., 2008. Estudio paleosismológico de la Falla de Carboneras: Evidencias tierra-mar de actividad tectónica reciente. GeoTemas 10, 1035-1038.

Pedrera, A., J. Galindo-Zaldívar, C. Marín-Lechado, F. J. García-Tortosa, P. Ruano, A. C. López Garrido, J. M. Azañón, J. A. Peláez, and F. Giaconia (2012a), Recent and active faults and folds in the central-eastern Internal Zones of the Betic Cordillera, J. Iber. Geol., 38(1), 191–208,http://dx.doi.org/10.5209/rev_JIGE.2012.v38.n1.39213 .

Pedrera, A., C. Marín-Lechado, D. Stich, A. Ruiz-Constán, J. Galindo-Zaldívar, C. Rey-Moral, and F. de Lis Mancilla (2012b), Nucleation, linkage and active propagation of a segmented Quaternary normal-dextral fault: the Loma del Viento fault (Campo de Dalías, Eastern Betic Cordillera, SE Spain), Tectonophysics, 522-523, 208–217. http://dx.doi.org/10.1016/j.tecto.2011.12.001.

Pedrera, A., Mancilla, F.D.L., Ruiz-Constán, A., Galindo-Zaldívar, J., Morales, J., Arzate, J., Marín-Lechado, C., Ruano, P., Buontempo, L., Anahnah, F., Stich, D., 2010. Crustal-scale transcurrent fault development in a weak-layered crust from an integrated geophysical research: Carboneras Fault Zone, eastern Betic Cordillera, Spain. Geochem. Geophys. Geosyst. 11(12). http://dx.doi.org/ 10.1029/2010gc003274.

Pedrera, A., Marín-Lechado, C., Galindo-Zaldívar, J., Rodríguez-Fernández, L.R., Ruiz-Constán, A., 2006. Fault and fold interaction during the development of the Neogene-Quaternary Almería-Níar basin (SE Betic Cordilleras), Geol. Soc. Spec. Pub., pp. 217-230. http://dx.doi.org/ 10.1144/GSL.SP.2006.262.01.13.

Pérouse, E., Vernant, P., Chéry, J., Reilinger, R., McClusky, S., 2010. Active surface deformation and sub-lithospheric processes in the western Mediterranean constrained by numerical models. Geology 38(9), 823-826. http://dx.doi.org/ 10.1130/G30963.1.

Reicherter, K., Hübscher, C., 2007. Evidence for a seafloor rupture of the Carboneras Fault Zone (southern Spain): Relation to the 1522 Almería earthquake? J. Seismol. 11(1), 15-26. http://dx.doi.org/10.1007/s10950-006-9024-0.

Reicherter, K.R., Reiss, S., 2001. The carboneras fault zone (Southeastern Spain) revisited with ground penetrating radar - Quaternary structural styles from high-resolution images. Geologie en Mijnbouw/Netherlands Journal of Geosciences, 80(3-4), 129-138.

Reilinger, R., McClusky, S., Vernant, P., Lawrence, S., Ergintav, S., Cakmak, R., Ozener, H., Kadirov, F., Guliev, I., Stepanyan, R., Nadariya, M., Hahubia, G., Mahmoud, S., Sakr, K., ArRajehi, A., Paradissis, D., Al-Aydrus, A., Prilepin, M., Guseva, T., Evren, E., Dmitrotsa, A., Filikov, S.V., Gomez, F., Al-Ghazzi, R., Karam, G., 2006. GPS constraints on continental deformation in the Africa-Arabia-Eurasia continental collision zone and implications for the dynamics of plate interactions. J. Geophys. Res. 111(B5), 26. http://dx.doi.org/10.1029/2005JB004051.

Rodríguez-Escudero, E., Martínez-Díaz, J.J., Álvarez-Gómez, J., Insua-Arévalo, J.M., Capote del Villar, R., 2013. Tectonic setting of the recent damaging seismic series in the Southeastern Betic Cordillera, Spain. Bull. Earthquake Eng. 12, 1-24. http://dx.doi.org/10.1007/s10518-013-9551-3.

Rutter, E.H., Faulkner, D.R., Burgess, R., 2012. Structure and geological history of the Carboneras Fault Zone, SE Spain: Part of a stretching transform fault system. J. Struct. Geol. 45, 68-86. http://dx.doi.org/10.1016/j.jsg.2012.08.009.

Sanz de Galdeano, C., Rodriguez Fernandez, J., López Garrido, A.C., 1985. A strike-slip fault corridor within the Alpujarra Mountains (Betic Cordilleras, Spain). Geol. Rundsch. 74, 641-655. http://dx.doi.org/ 10.1007/BF01821218.

Sanz de Galdeano, C., Shanov, S., Galindo-Zalívar, J., Radulov, A., Nikolov, G., 2010. A new tectonic discontinuity in the Betic Cordillera deduced from active tectonics and seismicity in the Tabernas Basin. J. Geodyn. 50(2), 57-66. http://dx.doi.org/10.1016/j.jog.2010.02.005.

Serpelloni, E., Vannucci, G., Pondrelli, S., Argnani, A., Casula, G., Anzidei, M., Baldi, P., Gasperini, P., 2007. Kinematics of the western Africa-Eurasia plate boundary from focal mechanisms and GPS data. Geophys. J. Int. 169(3), 1180-1200. http://dx.doi.org/10.1111/j.1365-246X.2007.03367.x.

Shen, Z.K., King, R.W., Agnew, D.C., Wang, M., Herring, T.A., Dong, D., Fang, P., 2011. A unified analysis of crustal motion in Southern California, 1970-2004: The SCEC crustal motion map. J. Geophys. Res. 116(B11), B11402. http://dx.doi.org/10.1029/2011jb008549.

Soto, J.I., Fernández-Ibáñez, F., Fernández, M., García-Casco, A., 2008. Thermal structure of the crust in the Gibraltar Arc: Influence on active tectonics in the western Mediterranean. Geochem. Geophys. Geosyst. 9(10), 27. http://dx.doi.org/10.1029/2008GC002061.

Stich, D., Ammon, C.J., Morales, J., 2003a. Moment tensor solutions for small and moderate earthquakes in the Ibero-Maghreb region. J. Geophys. Res. 108(B3), 1972-2012. http://dx.doi.org/10.1029/2002JB002057.

Stich, D., Batlló, J., Morales, J., Macià , R., Dineva, S., 2003b. Source parameters of the MW= 6.1 1910 Adra earthquake (southern Spain). Geophys. J. Int. 155(2), 539-546. http://dx.doi.org/10.1046/j.1365-246X.2003.02059.x.

Stich, D., Martín, R., Morales, J., 2010. Moment tensor inversion for Iberia-Maghreb earthquakes 2005-2008. Tectonophysics 483, 390-398. http://dx.doi.org/10.1016/j.tecto.2009.11.006.

Stich, D., Serpelloni, E., Mancilla, F., Morales, J., 2006. Kinematics of the Iberia-Maghreb plate contact from seismic moment tensors and GPS observations. Tectonophysics 426(3-4), 295-317. http://dx.doi.org/10.1016/j.tecto.2006.08.004.

Wessel, P., Smith, W.H.F., 1991. Free software helps map and display data. Eos Trans. AGU 72(41), 441. http://dx.doi.org/10.1029/90EO00319.

Williams, S., 2008. CATS: GPS coordinate time series analysis software. GPS Solutions 12(2), 147-153. http://dx/doi.org/10.1007/s10291-007-0086-4.

FIGURES

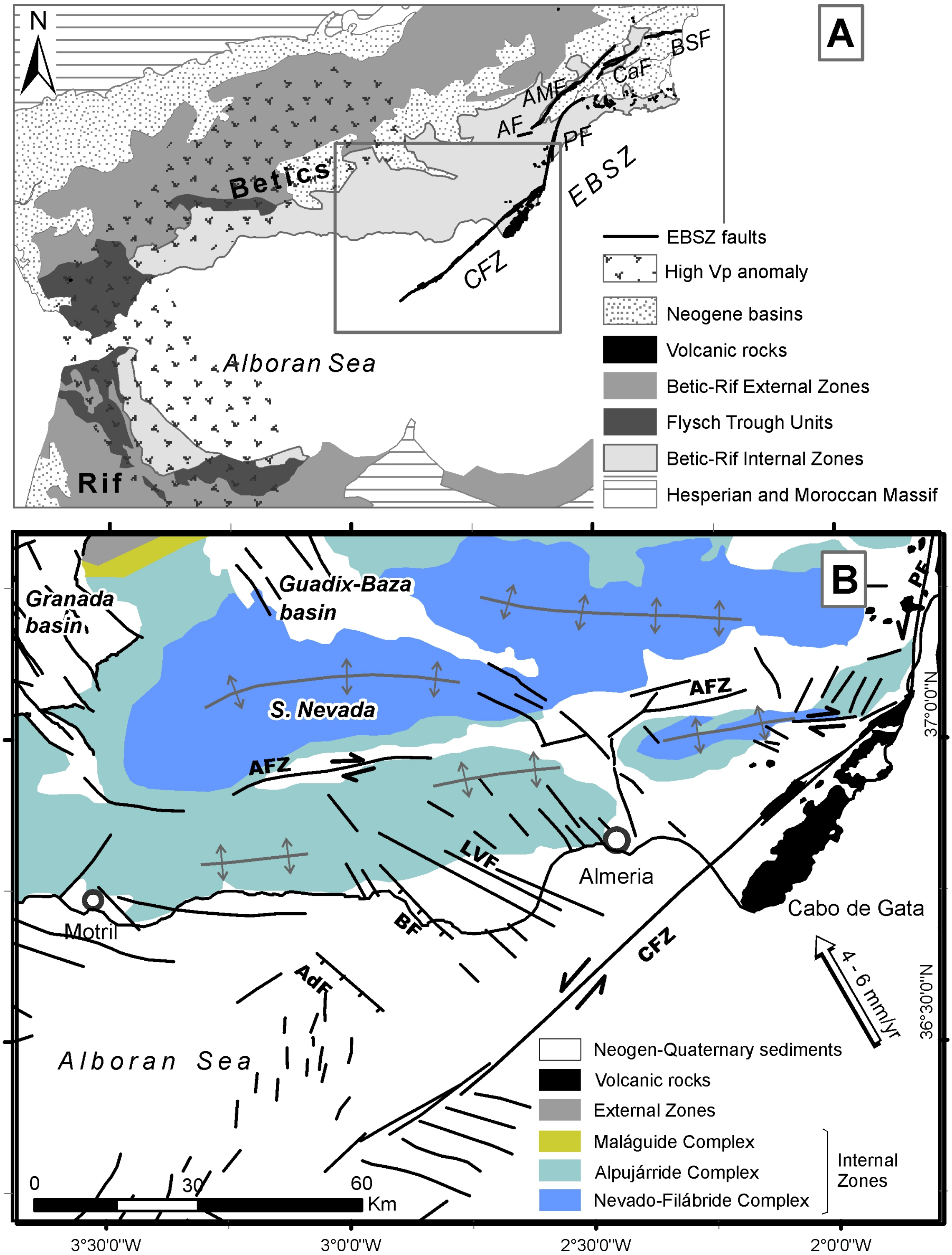

Figure 1. Simplified neotectonic map of the Betic-Rif arc. A) Regional setting. Arcuate shaped shaded region in Figure 1b indicates an approximate location of the high-velocity seismic anomaly at 135 km depth, according to the seismic tomography model (Bonnin et al., 2014). B) Study area. Quaternary active faults are from Gràcia et al. (2012) and QAFI database (García-Mayordomo et al., 2012), fold traces from Pedrera et al., (2012a). A thick arrow indicates a convergence between Nubia and Eurasia plates. Abbreviations: EBSZ: Eastern Betic Shear Zone; BSF: Bajo-Segura fault; CaF: Carrascoy fault, AMF: Alhama de Murcia fault; PF: Palomares fault;CFZ: Carboneras fault zone; BF: AFZ: Alpujarras fault zone; Balanegra fault; AF: Adra fault; LVF: Loma del Viento fault.

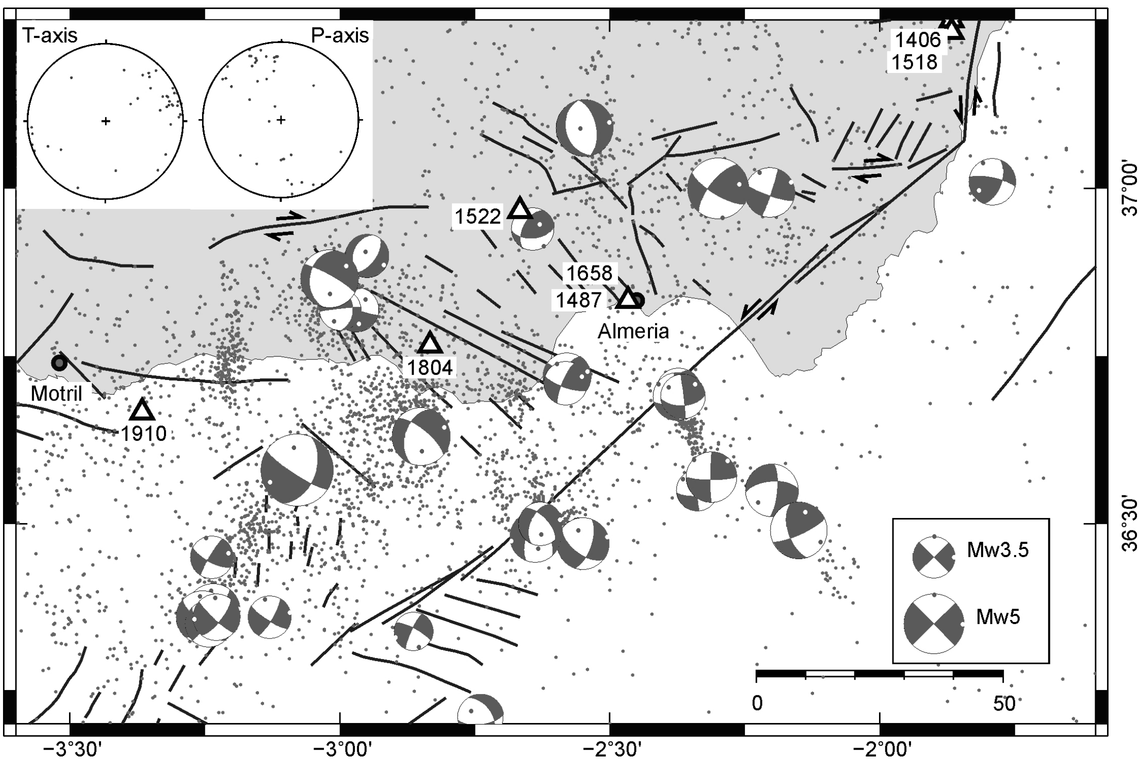

Figure 2. Seismotectonic map of the study area showing the seismicity from IGN catalogue (1926-2013) with depths ranging from 0 to 50 km (www.ign.es). Historical seismicity (white triangles) are from IGN catalogue and are labelled by the year of occurrence. P and T axes of the focal mechanisms (Table A1) are shown as grey and white dots, respectively. Stereographic projection of the P and T axes orientations for the displayed focal mechanisms are included in the upper left corner of the figure.

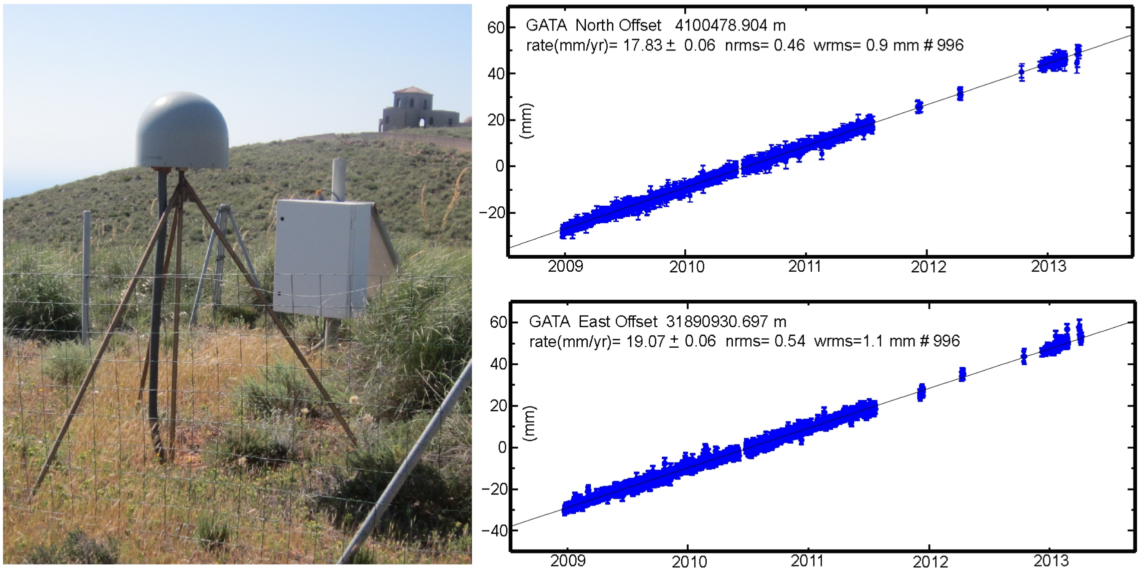

Figure 3. SDBM type monument and time-series of GATA CGPS station, installed in December of 2008. North-south (top) and east-west (bottom) components with 1σ errors are given in global ITRF2008 reference frame.

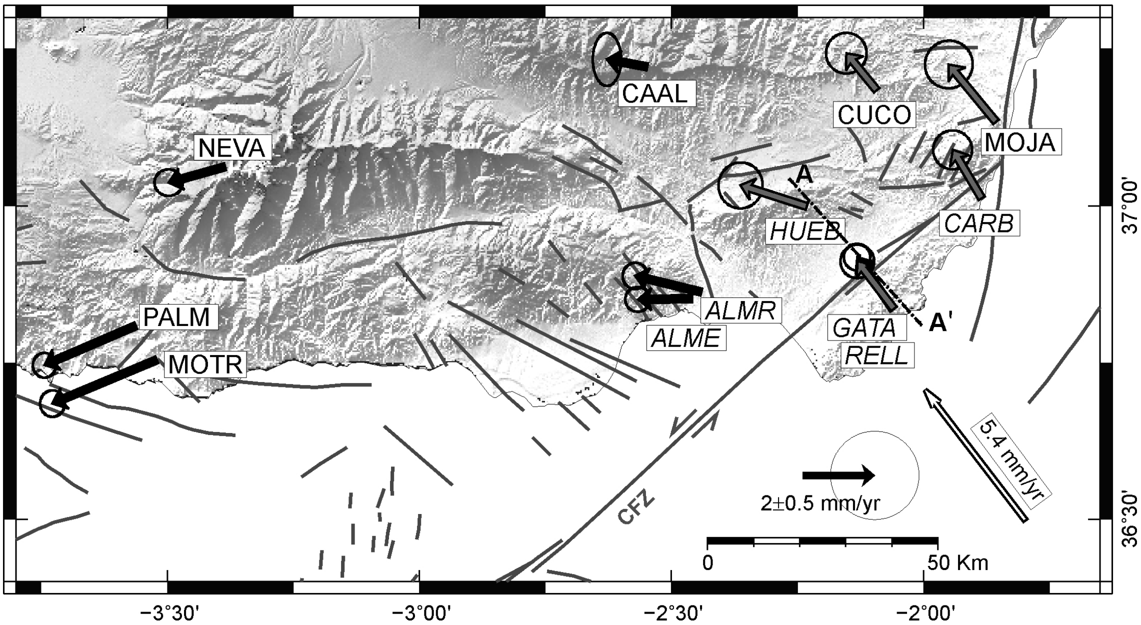

Figure 4. GPS velocities with 95% confidence error ellipses in western Europe reference frame. Plate convergence velocity from NNR-MORVEL56 model (Argus et al., 2011). CGPS and SGPS stations shown in black and dark grey, respectively. Stations included in A-A' profile (Figure 5) are marked by an asterisk.

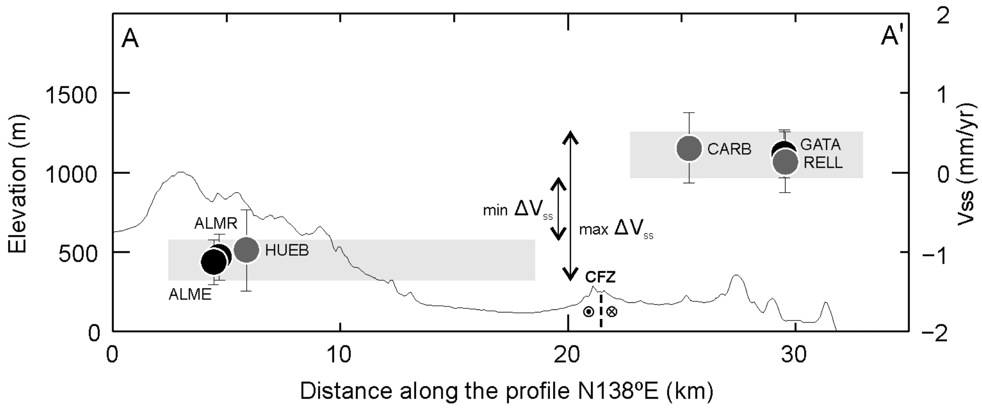

Figure 5. A-A' profile perpendicular GPS velocities with 1σ error bars. Location of the profile is shown in Fig. 4. Topography is represented with an irregular line on the bottom. ΔV_{ss} is the fault parallel strike-slip differential motion (velocity offset) between the two blocks. The intersection of the CFZ trace with the profile is shown as short dashed vertical line on the topographic profile.

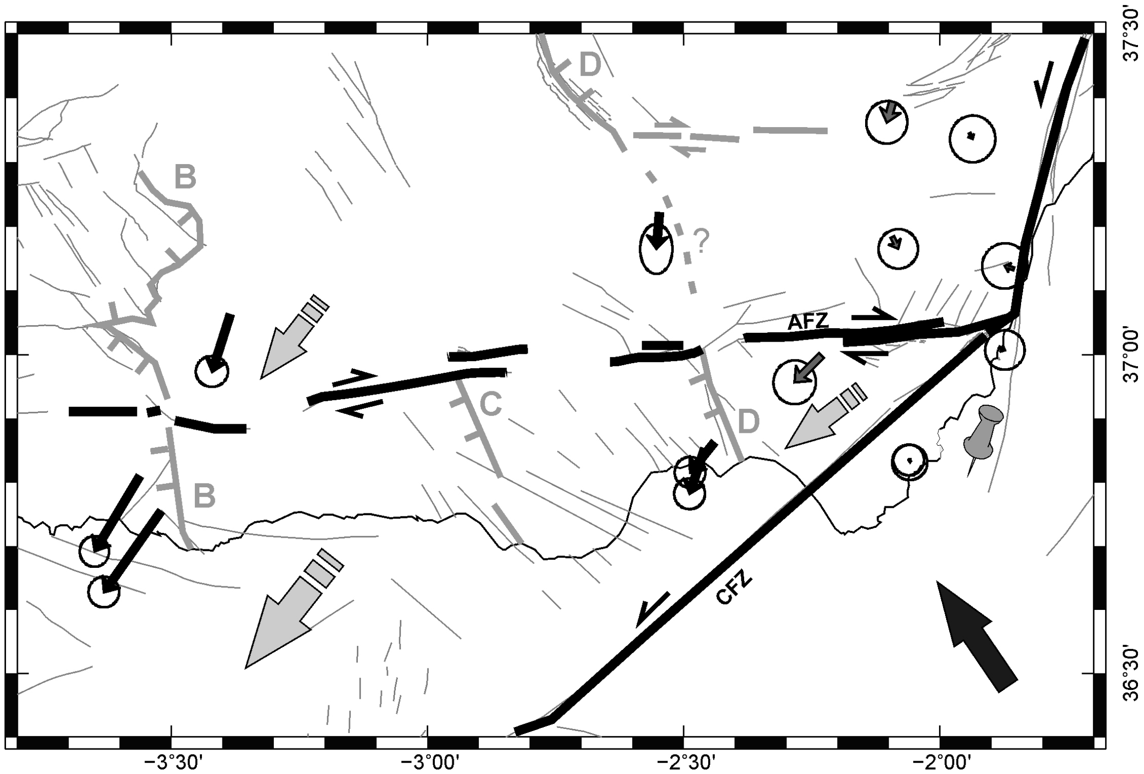

Figure 6. Map of the GPS horizontal velocities in GATA-fixed reference frame. Calculated strain rates determined at the centre of the 6 stations (marked by an asterisk) are shown as a white cross.

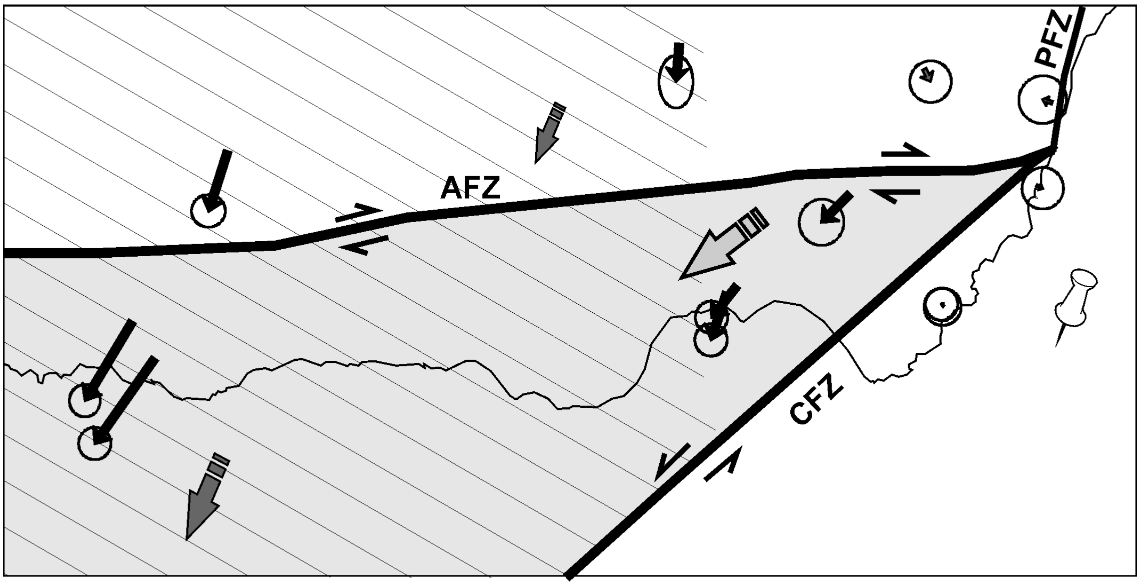

Figure 7. Simplified sketch of a proposed kinematic model. GPS velocities are given with respect to the GATA station. Block escape due to combined movement of CFZ and AFZ is shown in light gray. Striped area, extending to the east up to a longitude 2.5ºW and limited by the CFZ to the southeast, delimits an area possibly affected by deeper sub-lithospheric processes.

TABLES

Table A1. Compilation of focal mechanisms in the study area.

Long.	Lat.	Depth	Date	m_{rr}	m_{tt}	m_{pp}	m_{rt}	m_{rp}	m_{tp}	M_w	Ref.
(º)	(º)	(km)	dd/mm/yyyy	(dyn·cm)							
-3.08	36.58	16	16/06/1910	-3.50E+24	-7.20E+24	1.07E+25	-9.20E+24	3.50E+24	-6.30E+24	6.1	7
-2.15	36.49	12	06/01/1983	3.07E+22	6.23E+22	-9.29E+22	7.37E+22	6.90E+21	-8.76E+22	4.7	2
-2.2	36.55	6	20/03/1983	-1.28E+22	6.90E+21	5.90E+21	1.02E+22	-2.17E+22	4.26E+22	4.4	2
-2.3	37	9	13/09/1984	1.28E+23	-5.27E+23	4.00E+23	8.50E+22	-2.26E+23	-1.74E+23	5.1	1
-2.97	36.82	17	05/11/1986	-2.80E+20	1.48E+21	-1.20E+21	-3.62E+21	1.10E+21	1.95E+21	3.7	4

-3.02	36.87	-	23/12/1993	-5.90E+22	-4.10E+22	1.00E+23	1.50E+23	-6.60E+22	-7.50E+22	4.8	5
-2.85	36.63	-	04/01/1994	-1.11E+23	-7.10E+22	1.83E+23	1.36E+23	-4.80E+22	-8.00E+22	4.9	5
-3	36.82	10	18/05/1995	-2.30E+20	-1.00E+20	3.30E+20	1.70E+21	1.00E+20	1.42E+21	3.5	4
-2.95	36.9	4	13/12/1995	-2.79E+21	5.20E+20	2.27E+21	-1.07E+21	-8.90E+20	1.20E+21	3.6	4
-3.235	36.37	6	02/07/1997	-6.07E+21	-4.96E+22	5.57E+22	-2.82E+22	-7.57E+21	-8.28E+21	4.5	6
-3.255	36.36	10	02/07/1997	-3.63E+21	-3.96E+22	4.32E+22	-1.62E+22	-4.48E+21	-8.13E+21	4.4	6
-3.243	36.35	8	02/07/1997	-2.89E+20	-8.63E+21	8.92E+21	-3.42E+21	-2.99E+21	-4.66E+19	4	6
-3.229	36.36	10	03/07/1997	-4.72E+20	-8.57E+21	9.04E+21	-3.49E+21	6.54E+20	-1.31E+21	4	6
-3.238	36.45	16	07/08/1997	4.57E+20	-2.50E+21	2.04E+21	-2.38E+20	-8.68E+20	-1.32E+21	3.6	6
-1.792	37.01	8	06/04/1998	2.43E+21	-5.26E+21	2.83E+21	-3.71E+21	2.54E+21	-6.20E+21	3.9	6
-2.643	36.94	20	16/10/1998	1.94E+21	-1.67E+21	-2.67E+20	6.97E+20	-9.54E+20	-1.62E+21	3.6	6
-2.74	36.21	6	29/05/1999	-4.29E+21	5.53E+21	-1.24E+21	-2.74E+21	-2.13E+21	-3.93E+21	3.9	6
-3.131	36.36	16	27/05/2000	-4.62E+19	-2.59E+21	2.64E+21	-9.79E+20	-2.41E+20	-1.29E+21	3.6	6
-2.547	37.09	10	04/02/2002	-1.37E+23	1.13E+22	1.26E+23	1.07E+22	-5.91E+22	-2.78E+22	4.7	6
-2.204	36.99	12	06/02/2008	-1.75E+21	-1.15E+22	1.33E+22	-2.18E+21	-2.91E+21	-1.59E+22	4.2	8
-2.5	36.4	6	20/10/2008	-1.83E	-1.68E	3.50E+21	-1.07E	-2.18E	-2.27E	3.	8

5	7			+21	+21		+21	+21	+21	7	
-2.55	36.47	14	21/10/2008	-1.38E+21	-1.67E+22	1.81E+22	-7.94E+21	-1.22E+22	-2.03E+22	4.3	8
-2.55	36.47	14	21/10/2008	-5.14E+21	-1.88E+22	2.39E+22	-8.61E+21	-6.84E+21	-2.21E+22	4.3	8
-2.55	36.47	14	21/10/2008	-6.31E+20	-3.87E+21	4.50E+21	-1.86E+21	-4.81E+20	-4.24E+21	3.8	8
-2.55	36.47	14	26/10/2008	-1.44E+21	-8.41E+21	9.85E+21	-2.98E+21	-1.51E+21	-8.50E+21	4	8
-2.55	36.47	6	07/11/2008	-1.85E+22	-1.53E+22	3.38E+22	-1.81E+22	-9.28E+21	-1.61E+22	4.4	8
-2.312	36.57	8	05/07/2010	-3.59E+19	-4.46E+21	-4.50E+21	1.00E+21	-3.96E+21	-2.49E+22	4.2	3
-2.376	36.69	10	06/07/2010	2.16E+21	2.47E+21	-4.63E+21	2.35E+21	-4.73E+21	-1.09E+22	4	3
-2.365	36.69	12	06/07/2010	-2.40E+20	7.74E+20	-5.35E+20	1.52E+20	-2.35E+21	-3.50E+21	3.7	3
-2.338	36.55	8	10/07/2010	1.11E+20	3.00E+20	-4.11E+20	1.66E+20	-7.29E+20	-1.81E+21	3.5	3
-2.373	36.7	20	10/07/2010	1.97E+21	-2.69E+21	7.25E+19	1.65E+21	-1.60E+21	-2.42E+21	3.7	3
-2.582	36.71	26	12/10/2010	6.43E+20	-2.51E+21	1.87E+21	2.87E+20	-9.83E+20	-2.34E+21	3.7	3
-2.58	36.72	12	04/11/2010	-4.60E+20	-2.40E+21	2.86E+21	1.21E+21	-9.07E+20	-1.12E+21	3.6	3
-2.58	36.72	12	04/11/2010	-2.16E+20	-1.13E+22	1.15E+22	4.57E+21	-2.04E+21	-4.94E+21	4.1	3
-2.639	36.48	6	18/04/2012	-1.54E+22	-8.96E+21	2.44E+22	1.16E+22	6.46E+21	-7.18E+21	4.2	3
-2.629	36.5	6	18/04/2012	-1.72E+21	-1.28E+21	3.00E+21	1.63E+21	-2.07E+20	-7.47E+20	3.6	3

-2.864	36.34	9	14/08/2013	-3.10E+20	-5.35E+20	8.45E+20	1.07E+20	7.95E+19	-5.20E+20	3.3	9

References

[1] Buforn, E., Sanz de Galdeano, C. and Udías, A., 1995. Seismotectonics of the Ibero-Maghrebian region *Tectonophysics*, **248**, 247-261.

[2] Coca, P. and Buforn, E., 1994. Mecanismos focales en el sur de España: periodo 1965-1985 *Estudios Geológicos*, **50**, 33-45.

[3] Martín, R., Stich, D., Morales, J. and Mancilla, F., In this volume. Moment tensor solutions for the Iberian-Maghreb region during the Iberarray deployment (2009-2013) *Tectonophysics*.

[4] Martínez-Martínez, J.M., Booth-Rea, G., Azañón, J.M. and Torcal, F., 2006. Active transfer fault zone linking a segmented extensional system (Betics, southern Spain): Insight into heterogeneous extension driven by edge delamination *Tectonophysics*, **422**, 159-173.

[5] Stich, D., Alguacil, G. and Morales, J., 2001. The relative locations of multiplets in the vicinity of the Western Almería (southern Spain) earthquake series of 1993-1994 *Geophysical Journal International*, **146**, 801-812.

[6] Stich, D., Ammon, C.J. and Morales, J., 2003. Moment tensor solutions for small and moderate earthquakes in the Ibero-Maghreb region *Journal of Geophysical Research*, **108**.

[7] Stich, D., Batlló, J., Morales, J., et al., 2003. Source parameters of the MW= 6.1 1910 Adra earthquake (southern Spain) *Geophysical Journal International*, **155**, 539-546.

[8] Stich, D., Martín, R. and Morales, J., 2010. Moment tensor inversion for Iberia-Maghreb earthquakes 2005-2008 *Tectonophysics*, **483**, 390-398.

[9] http://www.ign.es/ign/layoutIn/sismoFormularioTensor.do

Table A2. Horizontal GPS velocities and 1σ uncertainties of the stations included in the study area are given in **bold** followed by the global stations used for defining a western Europe reference frame as used by Echeverria *et al.* (2013). *Ve*, *Vn* and *HorV, Az* are E-W, N-S and horizontal components of the GPS velocity vectors. *Rho* is the correlation between *Ve* and *Vn* and *1sig* are the 1σ uncertainties. Stations shown in bold letters refer to the GPS sites presented in Figures 4 and 6.

CODE	*Lat.*	*Long.*	*Ve*	*1sig*	*Vn*	*1sig*	*Rho*	*HorV*	*1sig*	*Az*
	(ºN)	*(ºE)*	*(mm/yr)*					*(mm/yr)*		*(ºN)*
ALME	-2.459	36.852	-1.5	0.1	0.0	0.1	0.000	1.50	0.14	269
ALMR	-2.441	36.863	-1.8	0.1	0.5	0.2	0.001	1.88	0.14	284
CAAL	-2.548	37.221	-1.1	0.2	0.2	0.3	0.000	1.14	0.17	281
CARB	-1.885	37.012	-0.8	0.2	1.4	0.2	0.003	1.57	0.22	329
CUCO	-2.093	37.184	-0.8	0.2	1.0	0.2	0.005	1.33	0.23	321
GATA	-2.061	36.835	-1.0	0.2	1.5	0.2	0.003	1.76	0.15	326
HUEB	-2.231	36.999	-1.8	0.3	0.6	0.3	0.008	1.93	0.25	288
MOJA	-1.856	37.134	-1.3	0.3	1.6	0.3	0.015	2.06	0.27	321

MOTR	-3.521	36.755	-2.9	0.1	-1.2	0.2	0.002	3.13	0.14	247
NEVA	-3.386	37.063	-1.6	0.2	-0.4	0.2	-0.001	1.62	0.16	254
PALM	-3.562	36.809	-2.5	0.1	-1.1	0.1	0.000	2.75	0.13	247
RELL	-2.059	36.836	-1.0	0.2	1.3	0.2	0.003	1.66	0.19	323
ALAC	-0.481	38.339	-0.4	0.2	0.3	0.1	0.009	0.50	0.14	312
CAGL	8.973	39.136	-0.5	0.1	0.5	0.1	-0.009	0.72	0.13	314
CASC	-9.418	38.693	-0.7	0.1	0.2	0.1	0.001	0.74	0.13	288
EBRE	0.492	40.821	-0.2	0.1	-0.1	0.2	0.000	0.24	0.14	242
GRAS	6.921	43.755	-0.2	0.1	0.0	0.1	0.005	0.16	0.13	259
GRAZ	15.493	47.067	0.3	0.2	0.5	0.2	0.020	0.61	0.19	32
HERS	0.336	50.867	-0.2	0.2	-0.2	0.2	0.006	0.28	0.19	215
LAGO	-8.668	37.099	-1.3	0.2	0.9	0.2	0.011	1.55	0.16	306
LPAL	-17.894	28.764	-3.6	0.2	0.4	0.2	0.071	3.57	0.16	276
MAS1	-15.633	27.764	-3.5	0.2	1.4	0.2	0.048	3.75	0.17	292
MATE	16.704	40.649	0.4	0.2	4.5	0.2	-0.013	4.54	0.16	5
MEDI	11.647	44.52	1.2	0.3	2.5	0.3	-0.001	2.75	0.26	26
ONSA	11.925	57.395	-0.6	0.2	-0.7	0.2	0.041	0.87	0.15	219
PDEL	-25.663	37.748	-3.2	0.2	0.4	0.2	0.020	3.20	0.20	276
POTS	13.066	52.379	-0.2	0.2	-1.1	0.2	0.074	1.07	0.17	192
RABT	-6.854	33.998	-3.7	0.1	1.7	0.1	0.005	4.02	0.14	294
SFER	-6.206	36.464	-3.3	0.1	0.6	0.1	0.001	3.32	0.12	281
TETN	-5.363	35.562	-4.9	0.2	0.6	0.2	0.011	4.94	0.16	277
TLSE	1.481	43.561	0.1	0.2	0.4	0.2	0.004	0.39	0.17	10
TORI	7.661	45.063	-0.7	0.5	-0.1	0.2	0.008	0.72	0.47	261
VILL	-3.952	40.444	-0.4	0.2	-0.4	0.2	0.000	0.62	0.16	224
WTZR	12.879	49.144	0.2	0.2	0.2	0.2	0.024	0.28	0.21	38
YEBE	-3.089	40.525	-0.5	0.1	-0.3	0.1	-0.001	0.59	0.13	238